Sensitivity of pollutants abatement in oxidation catalysts to the use of alternative fuels

Pedro Piqueras[a,*], María José Ruiz[a], José Martín Herreros[b], Athanasios Tsolakis[b]

[a] *CMT-Motores Térmicos, Universitat Politècnica de València, Camino de Vera s/n, 46022 Valencia, Spain.*
[b] *Deparment of Mechanical Engineering, University of Birmingham, Edgbaston B15 2TT, UK.*

Abstract

The aim to reduce well to wheel CO_2 emissions incentives the utilisation of alternative fuels (low to zero carbon content and/or low well to tank CO_2 emissions) as well as the enhancement of engine efficiency. In parallel, the reduction of engine tailpipe CO_2 emissions brings new challenges such as the decrease of the exhaust gas temperature. This trend penalises the ability of the exhaust aftertreatment system to eliminate pollutant emissions. In addition, the combustion of alternative fuels and new combustion modes induce changes in the nature and concentration of the exhaust species, which is known to affect the pollutants abatement mechanisms. This investigation provides new understanding on the sensitivity of pollutants abatement in oxidation catalysts to the use of alternative fuels. The studied fuels are conventional diesel, alternative fuels (rapeseed methyl ester and gas to liquid) as well as propane using a dual-fuel combustion strategy. The research combines experimental conversion efficiency from genuine exhaust gases with modelling work useful to explain the reasons for the change in light-off temperature as a function of the fuel. In addition to the CO and NO impact, HC surrogates are proposed distinguishing species of different reactivity for each fuel based on the experimental HC speciation. The results highlight the role of the engine-out emissions on the pollutants conversion efficiency. Their fashion with different fuels contributes to evidence the interest for low engine-out emissions along with low light alkanes content in total HC, as promoted by alternative fuels, to reduce the oxidation light-off temperature.

Keywords:
Internal combustion engine, Emissions, Alternative fuel, Oxidation catalyst, Conversion efficiency

1. Introduction

The demand of the society to reduce pollution is reflected in new tighten regulations that span the entire spectrum of human activities. As a consequence, the development of a wide variety of pollutant control technologies is promoted. As examples of their diversity, these techniques range from promising anodic oxidation for organic pollutants abatement from domestic sewage, agricultural runoff, industrial wastewater, and contaminated lands [1] to new

*Corresponding author. Tel.: +34 96 3877650, fax: +34 96 3877659.
Email address: pedpicab@mot.upv.es (Pedro Piqueras)

procedures for the environmentally friendly synthesis of catalysts used in photocatalytic degradation of pollutants in petroleum refinery effluents [2]. As a part of the need to respond to the pollutant control requirements in very different fields, new worldwide energy policies aim to highly reduce pollutant and greenhouse emissions from the transportation sector. To meet the requirements of the new regulations, the automotive industry is undergoing the electrification of the powertrain. Nonetheless, the improvement of the internal combustion engine is still necessary and shows promising technological advances [3]. One of the challenges to be faced is related to secondary effects of the engine thermal efficiency improvement. Although it governs the CO_2 emission reduction, the exhaust gas temperature is also decreased. Consequently, the pollutants conversion efficiency of the exhaust catalytic converters, whose main limiting factor to reach is the light-off temperature [4], is penalised and turns largely conditioned by the exhaust gas raw composition [5].

These drawbacks require to reduce the emissions from the source to minimise the aftertreatment system (ATS) requirements, with improved engine and ATS matching [6], optimisation of combustion strategies [7] and use of alternative cleaner fuels [8]. Low temperature combustion strategies have proved benefits in terms of engine-out NOx and soot emissions simultaneously, but CO and unburned HC mole fractions become several orders of magnitude higher than in conventional combustion [9]. To deal with these issues, dual mode concepts are being investigated as an approach to reduce CO_2 and regulated emissions [10] while allowing the utilisation of non-traditional fuels in transportation [11]. They can provide major reductions in pollutant emissions and contribute to the progressive decarbonisation of the internal combustion engines. Currently, the development status of alternative fuels (e.g. biodiesel, alcohols, and synthetic e-fuels) presents alternative-fuelled vehicles as a small but growing percentage of the EU's fleet. Market incentives, improvements in the implementation of the alternative fuels infrastructure and a more in depth understanding on the overall vehicle system efficiency and emissions improvements (e.g. post after-treatment tailpipe emissions) would catalyse their uptake.

In this line, alternative fuels have been also analysed to work with several engine concepts, such as conventional spark ignition [12], direct injection compression ignition [13], low temperature combustion strategies [14] and dual fuel concepts [15]. Nevertheless, more research is needed in alternative fuels [16] to reach an efficient market diffusion, being the first step a better definition of the most suitable fuels for decarbonization as a function of the market segment. Although alternative fuels have great potential [17], their research is still an emerging field and does not cover in detail all application sectors, such as heavy-duty vehicles [18], nor required technologies, such as specific aftertreatment systems [3], besides the impact of new policies, infrastructure development or commercial key markets [16]. In this context of further research efforts, biofuels like Rapeseed Methyl Ester (RME) and synthetic fuels such as Gas-to-Liquid (GTL), derived from a Fischer-Tropsch process have been shown as promising alternatives [19–21] in compression ignition engines. They are virtually free of sulphur and aromatic hydrocarbons, what can facilitate further reduction of engine-out emissions and improve the performance of the catalytic aftertreatment systems [22].

Despite these outcomes, the use of ATS is still needed to abate the pollutant emissions below the required limits. In particular, the oxidation catalyst manages the CO and total hydrocarbons (THC) abatement. Since the catalyst working principle is based on the contact of the species with the active sites, competition can appear between the different pollutants, thus damaging their conversion. The interactions between exhaust species have been extensively researched and modelled using synthetic mixtures of gases to represent the exhaust gas [23] and provide further understanding on the kinetic mechanisms [24]. Most of these works focus on tracing the behaviour of a reduced number of exhaust species with controlled composition [25]. However, the behaviour depends on the actual exhaust gas mixture [26]. The number of studies using real engine exhaust gas remains limited and focused on diesel fuel combustion [27]. In that sense, a large number of HC species with different reactivity are present, with a more varied spectrum in the case of non-traditional combustion [28]. In these cases, the flexibility of computational tools becomes essential to assist in the evaluation and understanding of the catalyst conversion efficiency.

This investigation provides new understanding on the correlation between genuine exhaust gas pollutant species from various fuels/combustion modes and the oxidation conversion efficiency of CO and THC via the combination of experimental and modelling work. The catalyst performance is studied under the use of conventional diesel combustion compared to alternative fuels (RME and GTL) as well as a dual fuel combustion mode with different diesel/propane ratios. Exhaust gas recirculation (EGR) was also considered in diesel-like fuels to reduce their NOx levels. Light-off tests were performed using a single cylinder diesel engine with a by-passed exhaust line towards the catalyst sample, placed inside a furnace to externally control a temperature ramp. Next, an oxidation catalyst model was developed to further understand the sensitivity of pollutants abatement to the use of alternative fuels through the determination of the kinetic properties of the CO and HC surrogates. The model comprises of CO and HC oxidation reactions, HC adsorption/desorption on zeolites, NOx redox reactions and the role of NO, CO and HC speciation on the oxidation inhibition terms. The HC surrogates distinguish the content of light and heavy species characterised by different reactivity. Therefore, the engine-out CO, THC and NO emissions as well as the relative content of HC species in THC are discussed as responsible of the trends in oxidation light-off temperatures as a function of the fuel and combustion strategy.

2. Materials and methods

In this section, the experimental setup and tests are firstly presented. Next, the oxidation catalyst model is described in detail.

2.1. Experimental setup and tests

A single-cylinder, naturally aspirated, direct injection, compression ignition engine was used as exhaust gas generator [29]. Table 1 summarises the main characteristics of the engine, whose exhaust line layout for this work is schematically shown in Figure 1.

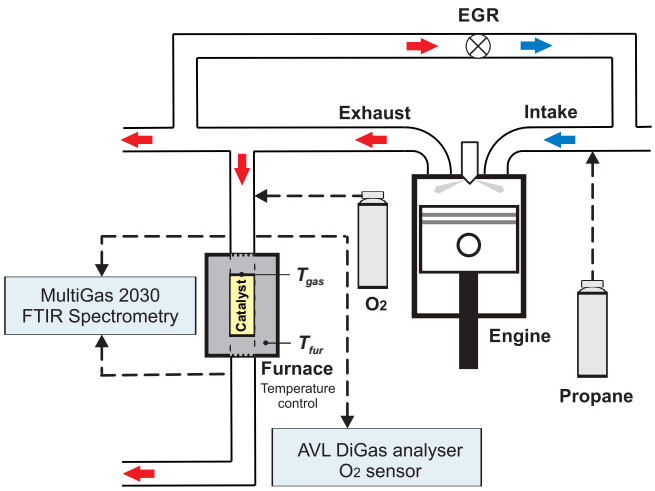

Figure 1: Scheme of the single-cylinder engine test cell.

The engine was equipped with a EGR system externally cooled, propane injection (for dual-fuel combustion mode) and O_2 injection at the catalyst inlet for accurate O_2 mole fraction control. From the exhaust ports, the exhaust gas was directed towards the oxidation catalyst with an exhaust gas space velocity of 35000 h^{-1}. The monolith, whose geometry is detailed in Table 2, was coated with Pt and Pd (1:1) over an alumina and zeolite washcoat. The catalyst was placed inside a furnace to impose the temperature independently of the engine operation. A K-type thermocouple was located at the catalyst inlet to measure the gas temperature along time. The gaseous emissions were measured using a MultiGas 2030 FTIR spectrometry analyser. The sampling line temperature was maintained at 150°C to avoid hydrocarbons and water condensation. The O_2 content was also measured using an AVL DiGas analyser fitted with an electrochemical O_2 sensor.

The engine was run at steady-state conditions at 1500 rpm and 40% in engine load. Six combustion cases were tested as a function of the fuel, combination of fuels (dual-fuel combustion) and EGR use. The main properties of the fuels used in the study, which were supplied by Shell Global Solutions UK, are summarised in Table 3. As baseline condition, the conventional diesel combustion mode was tested with ultra low sulphur diesel (ULSD) without EGR. This case will be referred as conventional diesel combustion (CDC) hereinafter. Next, diesel, RME and GTL were tested, but including EGR (25%) to reduce NOx emission while keeping comparable engine-out CO and HC emissions to the CDC. These cases are referred as CDC-EGR, RME-EGR and GTL-EGR respectively. Finally, dual-fuel combustion mode was considered using diesel as pilot fuel and propane, which was injected in the intake manifold in two percentages in volume of 0.2 % and 0.5 % (based on the volume of intake air replacement). As forward discussed in Section 3, these two cases resulted in huge engine-out CO and HC emissions but lower NOx than the conventional diesel combustion without EGR, so that EGR was omitted.

Table 1: Main characteristics of the engine.

Engine type	4 stroke, naturally aspirated
Number of cylinders [-]	1
Displaced volume [cm^3]	773
Stroke [mm]	101.6
Bore [mm]	98.4
Compression ratio [-]	15.5:1
Rated power [kW]	8.6 @ 2500 rpm
Maximum torque [Nm]	39.2 @ 1800 rpm
Injection system	Three hole direct injection
Engine piston	Bowl-in-piston

Table 2: Main data of the oxidation catalyst.

Diameter [m]	0.025
Length [m]	0.091
Cell density [cpsi]	400
Channel width [mm]	1.161
Wall thickness [mm]	0.109
Cell shape [−]	Square
Substrate material	Cordierite
Washcoat material	Alumina & zeolite
Washcoat loading [g/in^3]	2.6
PGM loading [g/ft^3]	120
Pt:Pd ratio [−]	1:1

As common boundary conditions for all tests, the temperature and O_2 content were set at the catalyst inlet. During the engine steady-state operation, the furnace imposed a heating temperature ramp of 2°C/min from 50°C to 380°C. In parallel, the O_2 content at the catalyst inlet was adjusted to 15% in mole fraction, as in conventional diesel combustion without EGR. Although O_2 is in excess in all cases to completely abate CO and HC emissions, keeping it equal avoided any sensitivity effect to this boundary condition on the conversion efficiency.

2.2. Oxidation catalyst model

An oxidation catalyst model based on the proposed by Piqueras *et al.* in [30] was developed by adapting to the particularities of this study. For the sake of completeness, the basis and main features of the model are described next. The model applies a lumped approach, so that constant flow properties are assumed along the monolith length. The

Table 3: Properties of the fuels used in the study.

	Liquid fuels			Gaseous fuel
Property	ULSD	RME	GTL	Propane
Cetane number	53.9	54.7	80	< 0
Density [kg/m^3]	827.1	883.7	784.6	1.5*
LHV [MJ/kg]	42.7	37.4	43.9	46.3
Sulphur [mg/kg]	46	5	< 10	0
Aromatics [%wt]	24.4	0	0.3	0
O [%wt]	0	10.8	0	0
C [%wt]	86.5	77.2	85	81.8
H [%wt]	13.5	12.0	15	18.2
H/C ratio (molar)	1.88	1.85	2.10	2.67
*15.6°C, 1 atm				

prediction of the flow properties at the catalyst outlet is performed from the mass flow and the inlet gas composition, pressure and temperature. Therefore, the outlet gas properties are obtained applying the energy and mass balances between inlet and outlet sections of the monolith as

$$T_{out} = \frac{c_{p,in}}{c_{p,out}} T_{in} - \frac{\dot{q}_{ht}}{\dot{m} c_{p,out}} + \frac{u_{in}^2 - u_{out}^2}{2 c_{p,out}} \tag{1}$$

$$u_{out} = \frac{A_{in} u_{in} p_{in} T_{out}}{A_{out} p_{out} T_{in}}, \tag{2}$$

where T, p, u, and c_p are referred to the gas temperature, pressure, velocity and specific heat at the inlet (in) and outlet (out) monolith cross-sections, whose areas are represented by A; $\dot{m}$ is the mass flow and $\dot{q}_{ht}$ stands for the exchange of thermal power between gas and substrate.

The outlet gas composition is determined from the inlet mass fraction and the variation of reactants and products according to the catalyst chemical mechanism:

$$Y_{k,out} = \frac{\dot{m}_{k,out}}{\dot{m}_{out}} = \frac{\dot{m}_{k,in} + \dot{m}_{in} \Delta Y_k}{\dot{m}_{in} \left(1 + \sum \Delta Y_i\right)} = \frac{Y_{k,in} + \Delta Y_k}{1 + \sum \Delta Y_i} \tag{3}$$

In Eq. (3), Y_k is the mass fraction of species k and $\dot{m}_k$ its mass flow at the inlet (in) and outlet (out) monolith cross-sections. Complementary, $\dot{m}$ is refered to the total mass flow at each cross-section and ΔY to the variation of mass fraction across the monolith.

The chemical kinetics is governed by the substrate temperature. This is calculated solving the general heat transfer equation by explicit centred finite differences. A lumped nodal scheme shown in Figure 2 was proposed to obtain the time variation of the substrate temperature taking into account that the tested monolith sample was inserted within a furnace and surrounded by its inner surface:

$$\Delta T_w = \frac{\Delta t}{C_w}\left(\frac{T_{gas,in} - T_w}{R_{gas,w}} + \frac{T_{fur} - T_w}{R_{rad}} + \dot{q}_r\right), \tag{4}$$

In Eq. (4), T_w is the substrate temperature; T_{gas} and T_{fur} are the boundaries and represent the catalyst inlet gas temperature and the furnace temperature respectively. The term C_w represents the thermal capacitance of the substrate and the washcoat; R is the equivalent thermal resistance, which accounts for convection between gas and substrate ($R_{gas,w}$) and radial conduction across the substrate cross-section (R_{rad}) [31]. Finally, $\dot{q}_r$ stands for the thermal power released by the chemical reactions.

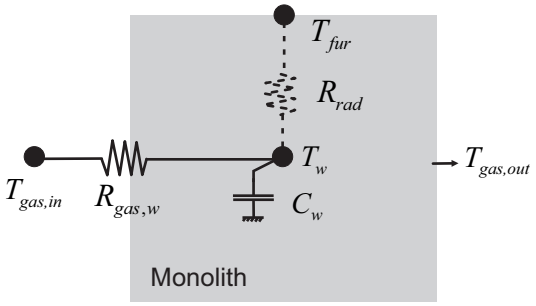

Figure 2: Lumped nodal scheme of the heat transfer sub-model.

The species conversion and the thermal power released is obtained by solving the chemical species transport in the bulk gas and the washcoat for the pollutant species along the monolith. Assuming quasi-steady flow, the transport equations for species n can be expressed as [32]:

$$u_{in}\frac{\partial X_n}{\partial x} = -S_{p,gas}k_{m,n}\left(X_n - X_{n,wc}\right) \tag{5}$$

$$\sum_i \nu_{i,n}R_i + S_{p,wc}k_{m,n}\left(X_n - X_{n,wc}\right) = 0 \tag{6}$$

The bulk-gas transport equation (Eq. (5)) describes the convective transport of the species along the monolith channels and its diffusion towards the washcoat interface. The diffusion term depends on the gas specific surface ($S_{p,gas}$), which is defined as the catalyst surface to gas volume ratio, and the mass transfer coefficient (k_m), which is computed as

$$k_{m,n} = \frac{D_{m,n}\mathrm{Sh_n}}{D_h}, \tag{7}$$

where D_h is the hydraulic diameter of the monolith channel, $\mathrm{Sh_n}$ is the Sherwood number of species n and $D_{m,n}$ represents the molecular diffusivity of species n in the exhaust gas obtained from the binary molecular diffusivity [33]:

$$D_{m_{n,k}} = \frac{0.0143T^{1.75}\sqrt{\frac{M_n+M_k}{M_nM_k}}}{\sqrt{2000}p\left(v_n^{\frac{1}{3}}+v_k^{\frac{1}{3}}\right)^2} \rightarrow D_{m,n} = \left(\sum_i \frac{X_i}{D_{m_{n,i}}}\right)^{-1} \tag{8}$$

Eq. (6) represents the chemical species transport in the washcoat, which balances the diffusion from the washcoat surface to its internal volume considering the washcoat specific surface ($S_{p,wc}$) and the reaction rate. The last is defined by the summation of the individual reaction rate of every reaction in which the species n is involved. The reaction mechanism considered in this work is listed in Table 4. The oxidation reactions of CO and HC are completed with the HC adsorption/desorption on zeolites besides the NOx redox reactions. HC reactions are distinguished for the different species composing the HC surrogate of each fuel, as discussed forward in Section 3.

The reaction rate is a function of several parameters. The main one is the intrinsic kinetic constant related to each reaction of the pollutant species n ($k_{r,n}$). It is defined as an Arrhenius type equation dependent on the substrate temperature. The CO and HC oxidations as well as the NOx redox reactions are also affected by an inhibition term ($G_{ox,n}$ [34] and $G_{redox,NOx}$ [35]), which considers the limitations on the reaction rate caused by the chemisorption of the species on the active sites. Although both CO and HC-i inhibition terms share the same expression, their coefficients K_j, which are defined as an Arrhenius expression, are distinguished for every pollutant in this work. In addition, the terms K_2 and K_3 are specified for each HC-i mole fraction separately. This way, the role of the HC speciation on the inhibition is considered. Concerning the sorption processes, the reaction rate depends on the surface coverage (θ) and the storage capacity per unit of volume (ψ).

To obtain the tailpipe emission, the differential equation system composed by Eqs. (5)-(6) was solved for each pollutant species. Taking into account that the gas phase and HC adsorption reactions are first order reactions with respect to species n and that the HC desorption is a zero order reaction, the system has a explicit solution assuming constant O_2 concentration ($X_{O_2} = 15\%$) [30]. In a general way, this is expressed as

$$X_{n,gas,out} = \frac{\left((1-a_n)\,X_{n,gas,in} - b_n\right)e^{-S_{p,gas}k_{m,n}(1-a_n)\tau} + b_n}{(1-a_n)} \tag{9}$$

where τ is the residence time of the gas and the terms a_n and b_n are constants within the control volume. Dividing the reaction rate of the first order reactions into the washcoat concentration of species n ($R^{1'}_{j,n}$), a_n and b_n are defined as:

Table 4: Reaction mechanism of the oxidation catalyst model.

Reaction	Reaction rate
CO oxidation: $CO + \frac{1}{2}O_2 \rightarrow CO_2$	$R_{ox,CO} = \frac{k_{ox,CO}}{G_{ox,CO}} X_{O_2} X_{CO,wc}$
HC-i oxidation: $C_nH_m + \left(n + \frac{m}{4}\right) O_2 \rightarrow nCO_2 + \frac{m}{2}H_2O$	$R_{ox,HC-i} = \frac{k_{ox,HC-i}}{G_{ox,HC-i}} X_{O_2} X_{HC-i,wc}$
HC-i adsorption & desorption: $C_nH_m + Zeol. \rightleftarrows C_nH_m \bullet Zeol.$	$R_{ads,HC-i} = k_{ads,HC-i}\,(1 - \theta_{HC-i})\,\psi_{HC-i} X_{HC-i,wc}$
	$R_{des,HC-i} = k_{des,HC-i} \theta_{HC-i} \psi_{HC-i}$
NOx redox: $NO + \frac{1}{2}O_2 \rightleftarrows NO_2$	$R_{ox,NO} = \frac{k_{ox,NO}}{G_{redox,NOx}} X_{NO,wc} \sqrt{X_{O_2}}$
	$R_{red,NO_2} = \frac{k_{red,NO_2}}{G_{redox,NOx}} X_{NO_2,wc}$
Inhibition term	
$G_{ox,n} = T_w \left(1 + K_{1,n} X_{CO,wc} + \sum_i \left(K_{2,n,HC-i} X_{HC-i,wc}\right)\right)^2 \left(1 + X_{CO,wc}^2 \sum_i \left(K_{3,n,HC-i} X_{HC-i,wc}{}^2\right)\right)^2 \left(1 + K_{4,n} X_{NO,wc}^{0.7}\right)$	
$G_{redox,NOx} = 1 + K_{1,NOx} + K_{2,NOx} \sqrt{X_{O_2}} + K_{3,NOx} X_{NO_2,wc}$	

$$a_n = \frac{S_{p,wc} k_{m,n}}{S_{p,wc} k_{m,n} - \sum_j \nu_{j,n} R_{j,n}^{1'}} \tag{10}$$

$$b_n = \frac{\sum_i \nu_{i,n} R_i^0}{S_{p,wc} k_{m,n} - \sum_j \nu_{j,n} R_{j,n}^{1'}} \tag{11}$$

Finally, applying the stoichiometry of every reaction, the heat released is calculated as summation of the oxidation and sorption reactions contribution:

$$\dot{q}_r = \dot{n}_{gas} \sum_j H_{f,j} \Delta X_j + \Psi_{HC} \sum_i \Delta H_{HC-i,\frac{ads}{des}} \frac{\Delta \theta_{HC-i}}{\Delta t} \tag{12}$$

The term $\dot{n}_{gas}$ represents the total exhaust gas mole flow entering the catalyst, $H_{f,j}$ is the enthalpy of formation of the species j and ΔX_j its mole fraction variation due to the gas phase reactions. In the second term, which concerns the

adsorption/desorption of hydrocarbons, $\Delta H_{HC-i,\frac{ads}{des}}$ is the heat of adsorption/desorption of HC species in the zeolites and $\Delta\theta_{HC-i}$ is the HC coverage variation.

3. Results and discussion

The use of different fuels and combustion strategies determined the exhaust gas composition. Figure 3 shows the experimental engine-out emissions of CO, THC and NOx (distinguishing NO and NO_2) for the tested cases. The NOx emissions are mostly sensitive to the usage of EGR, despite a minor influence of the fuel. At first glance, the combustion cases with EGR presented lower NOx emission than CDC. In particular, the reduction in NOx was basically given by the decrease of the NO emission. The minimum NOx emission was found for GTL-EGR. The dual-fuel combustion cases combining diesel and propane, which were tested without EGR, showed the same NOx emission as CDC. However, a shift from NO to NO_2 was observed, increasing the NO_2 to NOx ratio from 10% in CDC to 35%.

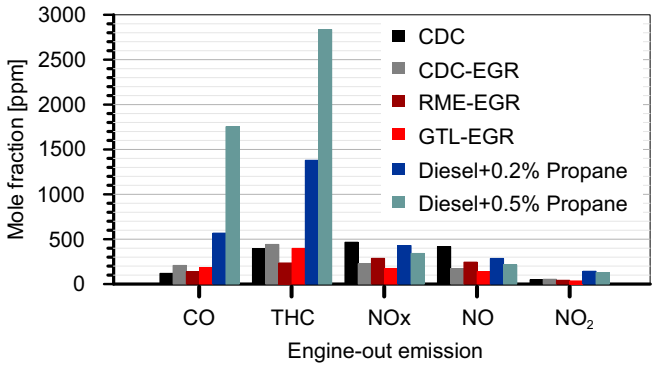

Figure 3: Gaseous engine-out emissions as a function of the combustion case.

Regarding CO emissions, the lowest value corresponded to CDC. When EGR was employed, the CO emission slightly increased for every fuel (CDC-EGR, RME-EGR and GTL-EGR). The engine-out THC emission showed less sensitivity to EGR and even a decrease was obtained in RME-EGR case with respect to CDC.

However, a significant increase of CO and THC was observed in dual-fuel combustion mode. In the case of diesel and 0.5% propane, the engine-out CO emission was increased 15 times, whilst THC did 7 times, with respect to CDC. Besides the huge increase in THC, the HC speciation also changed entirely, as depicted in Figure 4.

The main species in THC for diesel and alternative fuel combustions were medium-heavy HCs. Their presence ranged from 64.5% to 72.2%. By contrast, this group was minority in dual-fuel combustion based on propane addition to diesel. In the two tested cases, the medium-heavy HC content in THC was reduced to around 10%, with lower presence as the propane content increased. Complementary, the light HC species represented most of the engine-out THC emission in the dual-fuel combustion cases. In particular, propylene and propane were the most present HC

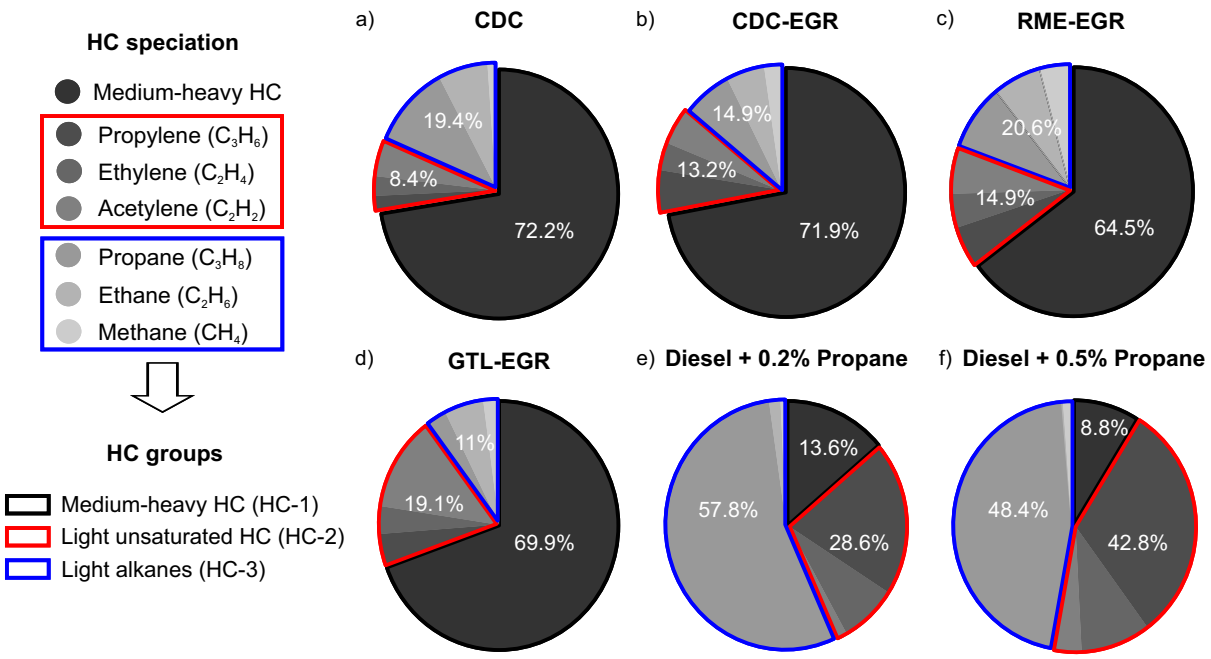

Figure 4: HC speciation of engine-out emissions for every combustion case and definition of HC groups for modelling proposals.

species. Although this result was expected, it is worth to note that in diesel and alternative fuel cases, the content of the compounds composing the light HC species was more homogeneous than in diesel-propane combustion. Based on these results, the HC input in the model was defined considering three main HC groups:

- Medium-heavy HCs (HC-1)
- Light unsaturated HCs (HC-2): propylene, ethylene, acetylene
- Alkanes light HCs (HC-3): propane, ethane, methane

These groups enabled representing the individual oxidation and adsorption properties of the species present in the actual exhaust gas. The content of these groups in every THC, which is indicated in Figure 4, defined the HC surrogate for every fuel and combustion case. A HC compound was selected to emulate the physical and chemical properties of every group in the model. The medium-heavy HCs group was represented by decane, a majority HC species in compression ignition combustion with diesel in conventional [36, 37] and dual-fuel strategies [28]. Decane is commonly considered in the literature to represent heavy, adsorbable, hard-to-oxidise HCs [35]; the reactivity of light HC species was modelled using propylene (HC-2) and propane (HC-3) as high reactivity (unsaturated) and low reactivity (saturated) light HCs respectively. This choice is justified by its presence in CDC, CDC-EGR, RME-EGR and GTL-EGR exhaust gases along with its majority content in diesel-propane duel-fuel combustion (Figure 4). The main characteristics of the HC species considered in the model are summarised in Table 6 [38]. The relevant properties concern the molecular weight, the diffusion volume, the critical temperature and the heat of formation. The diffusion

volume is used to compute the molecular diffusivity (Eq. (8)) and was calculated according to the correlation proposed by Poling [33] for hydrocarbons (C_nH_m):

$$\upsilon = 15.9n + 2.31m \tag{13}$$

The critical temperature and the heat of formation are required to calculate the thermal power released by the chemical reactions. The heat of adsorption-desorption was defined as a function of the critical temperature as [39]:

$$\Delta H_{\frac{ads}{des},HC-i} = 74380e^{-0.3238\frac{T_w}{T_{c,HC-i}}}\left(1 - \frac{T_w}{T_{c,HC-i}}\right)^{0.3238} \tag{14}$$

and the heat of formation of every HC species was determined according to the correlation shown in Eq. (15), whose coefficients are listed in Table 6 for every species. These were obtained from enthalpy data at different temperatures provided by [40] (decane and propane) and [41] (propylene).

$$\begin{aligned} H_{f,HC-i} = \Re\Big(a_{H_f,0,HC-i} + \frac{a_{H_f,1,HC-i}}{T_w} + a_{H_f,2,HC-i}T_w + \\ + a_{H_f,3,HC-i}T_w^2 + a_{H_f,4,HC-i}T_w^3 + a_{H_f,5,HC-i}T_w^4\Big) \end{aligned} \tag{15}$$

Table 5: Species to represent the characteristic HC groups composing the THC in the catalyst model.

Species	Description
HC-1 : $C_{10}H_{22}$	Medium-heavy HCs, adsorbable and medium reactivity
HC-2 : C_3H_6	Light unsaturated HCs, non-adsorbable and high reactivity
HC-3 : C_3H_8	Light alkanes, non-adsorbable and low reactivity

Table 6: Properties of HC species used in the catalyst model.

Variable	HC-1 ($C_{10}H_{22}$)	HC-2 (C_3H_6)	HC-3 (C_3H_8)
Molecular weight [g/mol]	142.28	42.08	44.1
Diffusion volume [m^3/mol]	209.82	61.56	66.18
Critical temperature [K]	617.8	365.2	369.9
$a_{H_f,0}$ [-]	-21558	4303	-8850
$a_{H_f,1}$ [-]	-2.7093×10^4	-1.5342×10^4	-8.6081×10^4
$a_{H_f,2}$ [-]	-3.6119×10^1	-6.0216×10^0	-1.4407×10^1
$a_{H_f,3}$ [-]	2.9563×10^{-2}	-1.4149×10^{-3}	9.6596×10^{-3}
$a_{H_f,4}$ [-]	-1.0088×10^{-5}	5.1305×10^{-6}	-1.7851×10^{-6}
$a_{H_f,5}$ [-]	1.3093×10^{-9}	-1.9011×10^{-9}	-2.7873×10^{-11}

3.1. CO light-off curves

The combination of experimental and modelling results confirms how the exhaust emission composition from each fuel-combustion mode configuration governs the oxidation performance of the catalytic converter. Figure 5 shows the CO conversion efficiency in the experimental and modelled light-off tests. Good agreement was obtained for the six combustion studied cases, with high accuracy around the light-off region with only some disagreements at very low temperature. In this range, the theoretical computation converges to null conversion efficiency whilst small experimental deviations can lead to spurious results. The setup of the chemical kinetic model is detailed in Table 7.

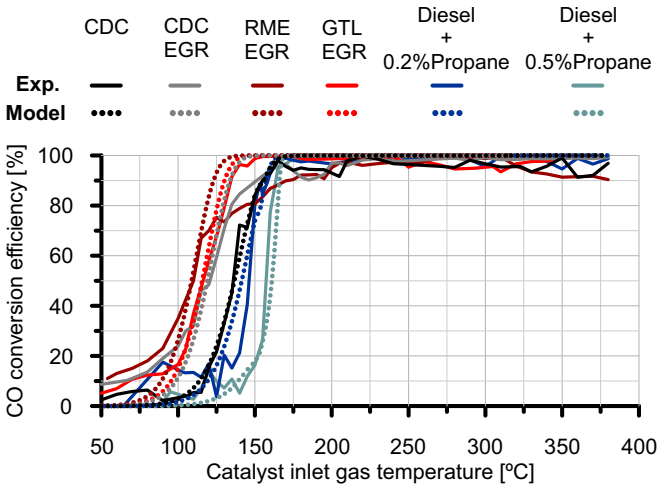

Figure 5: Experimental and modelled CO light-off curve as a function of the combustion case.

Compared to CDC, the use of EGR caused a relevant decrease of the CO light-off temperature ($T50_{CO}$). Taking as a basis for comparison the modelling results, CDC-EGR reduced the light-off temperature from 136°C (CDC) to 119°C. This positive trend was even improved by GTL-EGR and RME-EGR, which reached an earlier CO light-off (116°C and 109°C respectively). The reason for this response lies on the engine-out emission, previously presented in Figure 3. Besides the influence of the CO mole fraction on the oxidation rate (first-order reaction with respect to CO), the species competition is considered through the CO inhibition term, whose value is shown in Figure 6.

The CO inhibition term decreased monotonously with the temperature increase as a combination of its thermal dependence and the decrease of the CO and HCs washcoat mole fractions. This way, the temperature increase caused a snowball effect due to the progressively higher intrinsic kinetics and lower inhibition. Firstly focusing on conventional combustions, the CO inhibition term is correlated with the CO light-off temperature. CDC produced the highest inhibition, what explains the highest $T50_{CO}$ for this case. The inhibition term decreased in EGR combustions, progressively from diesel, GTL and RME as $T50_{CO}$ did.

Despite CDC was characterised by the lowest CO emission, the high engine-out THC and, specially, NO emissions with respect to cases with EGR (diesel and alternative fuels) resulted in higher inhibition for CDC. The trend in the

Table 7: Setup of the kinetic parameters in the oxidation catalyst model.

Kinetic constants		
	P_f [−]	E_a [J/mol]
CO oxidation	8×10^{17}	79000
$HC-1$ oxidation	8×10^{17}	95000
$HC-2$ oxidation	8×10^{18}	90000
$HC-3$ oxidation	1×10^{15}	100000
NO oxidation	2×10^{6}	30000
NO_2 reduction	1×10^{10}	87070
$HC-1$ adsorption	0.7	0
$HC-1$ desorption	100	105000
Inhibition terms		
	P_f [−]	E_a [J/mol]
$K_{1,CO}$	555	−7990
$K_{1,HC-i}$	555	−7990
$K_{1,NOx}$	3×10^{-8}	−81481
$K_{2,CO\&HC-2,HC-1}$	500	−3000
$K_{2,CO\&HC-2,HC-2}$	1000	−3000
$K_{2,CO\&HC-2,HC-3}$	500	−3000
$K_{2,HC-1\&HC-3,HC-1}$	1000	−3000
$K_{2,HC-1\&HC-3,HC-2}$	1000	−3000
$K_{2,HC-1\&HC-3,HC-3}$	10000	−3000
$K_{2,NOx}$	3×10^{-7}	−83143
$K_{3,CO\&HC-2,HC-i}$	0.5	−26534
$K_{3,HC-1\&HC-3,HC-1}$	10	−96534
$K_{3,HC-1\&HC-3,HC-2}$	10	−96534
$K_{3,HC-1\&HC-3,HC-3}$	100	−96534
$K_{3,NOx}$	6×10^{-7}	−9977
$K_{4,CO\&HC-2}$	1	−31036
$K_{4,HC-1\&HC-3}$	0.01	−31036

CO inhibition term shown in Figure 6 evidences how NO competes with CO for active sites. As observed, the CO inhibition was kept high in CDC, even as the temperature increased. However, the inhibition converged to a low value in the other tested cases. This behaviour was due to the penalty caused by the NO washcoat mole fraction. It was the

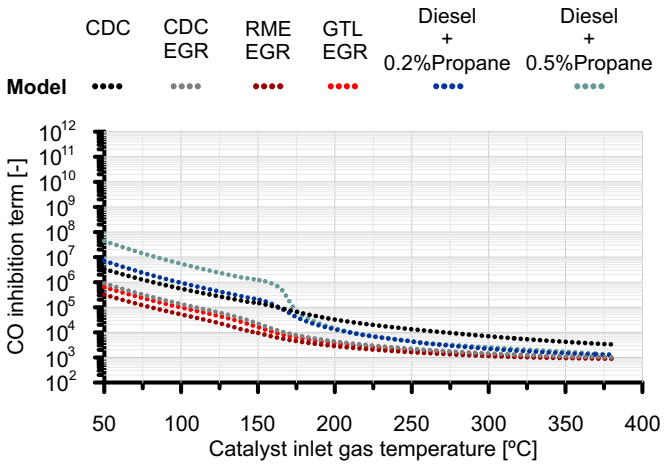

Figure 6: CO oxidation inhibition term as a function of temperature and combustion case.

highest one in CDC due to the highest engine-out NO emission in this combustion case. On the one hand, it affects at low temperature because of the kinetically limited reaction rate, which avoids the NO oxidation to NO_2. On the other hand, the NO oxidation is gradually frozen at high temperature due to the thermodynamic equilibrium. Therefore, NO is the maximum responsible of the high inhibition as the temperature increases, since similar CO and HC washcoat mole fraction is found in all cases due to the high conversion efficiency reached for these pollutants.

HCs, in addition to NO, were also participating in CO inhibition. Note that the engine-out THC emissions were comparable in diesel and alternative fuels. Nonetheless, the HC surrogate of the CDC contained the highest amount of medium (HC-1) and low (HC-3) reactivity HCs. Consequently, the HC washcoat mole fraction for CDC is expected to be higher than in combustions using EGR. This result is evidenced by the low THC conversion efficiency within the CO light-off window shown in Figure 7 for CDC, despite the HC adsorption. As a result, the higher THC washcoat mole fraction in CDC also contributed to higher CO inhibition term.

In contrast to EGR and alternative fuels, which benefit the CO light-off with respect to CDC, the dual-fuel combustion based on diesel and propane shifted the light-off to higher temperature. An increase in $T50_{CO}$ of 5°C was observed for diesel + 0.2% propane case compared to CDC. However, the delay reached 24°C for the diesel + 0.5% propane combustion. This sharp increase means a delay in CO light-off up to 52°C of diesel + propane combustion with respect to RME-EGR, i.e. a penalty of 47.7% in $T50_{CO}$.

The engine-out NO emission in dual-fuel combustion cases was lower than in CDC. Taking into account only this effect, the dual-fuel combustion cases should have exhibited a low inhibition term and obtained an earlier CO light-off. With this premise, the higher $T50_{CO}$ obtained by dual-fuel combustion cases can be exclusively attributed to the huge increase of the engine-out CO and THC emissions (increasing further as the injected propane did). This caused relevant both CO self-inhibition and competition with HC species [5]. Figure 6 shows that the CO inhibition term is one to two orders of magnitude higher in dual-fuel combustion cases than its counterpart for CDC and RME-EGR

till 175°C. The very marked decrease of the CO inhibition term with temperature for the dual-fuel combustion cases, especially in the 0.5% propane test, was due to the sharp decrease of CO and THC washcoat mole fraction related to the reactivity (conversion efficiency) increase. As high conversion efficiency is reached, the engine-out emissions loss weight to set the washcoat mole fraction for the reactant species. Consequently, the inhibition terms of all combustion cases tend to coincide.

3.2. THC light-off curves

The change in THC abatement as a function of the combustion-fuel case shares with CO the same roots regarding inhibition effects. However, the adsorption at low temperature and the variation of the THC speciation brought additional features to the fuel sensitivity. Figure 7 represents the THC conversion efficiency distinguishing the adsorption and oxidation contributions in separated charts. As for CO, the THC light-off curves were also modelled with good accuracy, correctly identifying the main trends in adsorption, light-off and maximum conversion efficiency. Nevertheless, the concurrence of adsorption and oxidation, as well as the complexity of the actual THC speciation and its idealisation in the model, brought some slight discrepancies. The most remarkable is the crossing between RME-EGR and GTL-EGR between 90°C and 145°C predicted by the model but not present in the experimental results.

At low temperature, the THC abatement is based on the accumulation on the zeolite, with a progressive increase of the oxidation rate as the temperature does. Although the model predicts properly the order of magnitude of the adsorption conversion efficiency and the main differences between the tested cases, this temperature range is the one showing the main deviations with respect to the experiments due to applied assumptions. The adsorption affects mainly to long chain HCs, which are more easily trap on zeolites due to the stronger Van der Waals forces [42, 43], as experimentally evidenced in Figure 8. For the sake of simplicity, the modelling of HC adsorption was considered only for medium-heavy HCs (HC-1). In addition, the variability in adsorption characteristics of all species composing this group was represented for just one species (decane). Hence, the source of deviations with respect to the experiments. Nevertheless, such simplifications are useful to make easier the understanding of the differences between every combustion-fuel case, as forward discussed.

As shown in Figure 7(b), the THC conversion efficiency due to adsorption was comparable among all single-fuel combustion cases. This was due to the similar amount of medium-heavy HCs. It resulted in an overall THC conversion efficiency around 50%, with a tendency to decrease as the temperature increased. It is interesting to note how CDC-EGR showed the highest rate of conversion efficiency decrease due to adsorption. This was due to the higher engine-out THC emission along with almost the same content in HC-1 (i.e. the higher engine-out HC-1 emission) than CDC and GTL-EGR cases. Consequently, faster increase of the HC surface coverage was obtained, thus slowing down the dynamics of the adsorption process with respect to the other cases. Since CDC and GTL-EGR provided the same engine-out HC-1 emission, the model provided basically identical THC adsorption conversion efficiency. Regarding RME-EGR, the initial THC adsorption efficiency was the lowest one of the single-fuel combustion cases, in agreement with its lowest engine-out HC-1 emission (due to the lowest engine-out THC emission and the lowest HC-1

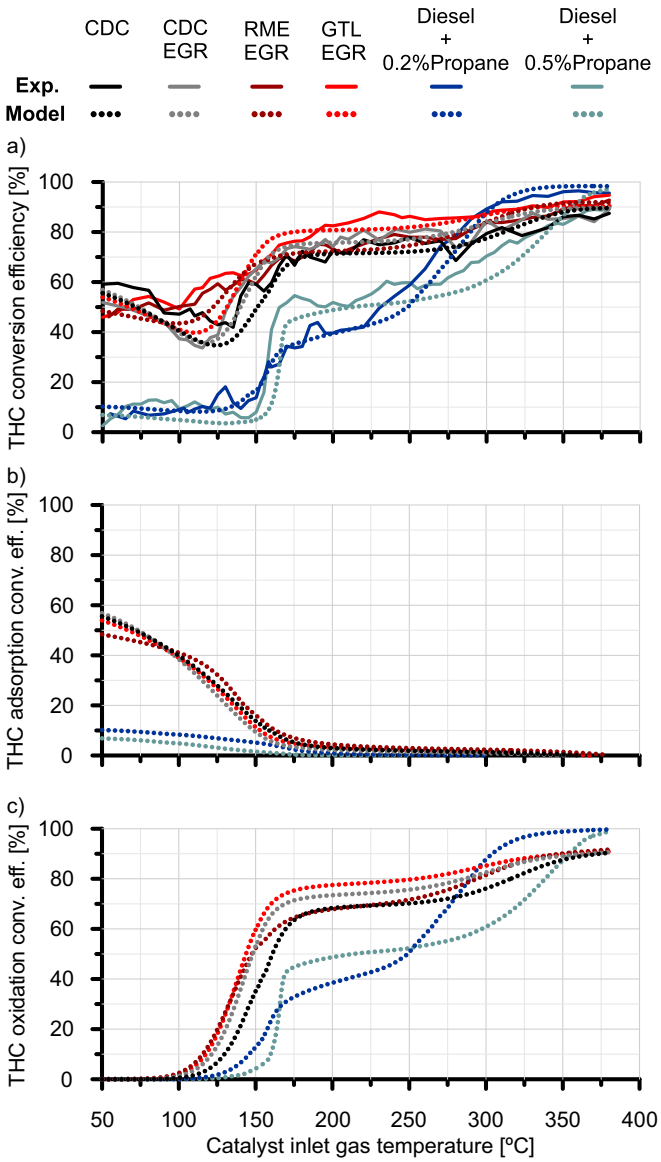

Figure 7: THC light-off curve as a function of the combustion case: (a) Comparison between experimental and modelled results, (b) THC conversion efficiency due to adsorption and (c) THC conversion efficiency due to oxidation.

content). This is positive in terms of adsorption dynamics, since the slower saturation of the zeolites provides less adsorption dependency on the temperature. This theoretical behaviour is the one responsible of the higher modelled RME-EGR THC conversion efficiency than in GTL-EGR case between 90°C and 145°C, opposite to experimental data. Nonetheless, these small experimental to model deviations are not relevant concerning the overall significance of the results. In fact, they contribute to underline the low relevance of experimental uncertainties and modelling simplifications on the obtained trends.

According to the results of the single-fuel combustion cases, the low medium-heavy HC (HC-1) content in alternative fuels also determined the trend of their THC adsorption conversion efficiency. In contrast to conventional combustion, the adsorption in dual-fuel combustion with 0.2% propane scarcely represented a 10% of THC removal. It became even lower when the injected propane was increased to 0.5% due to the further percentage reduction of HC-1 content in THC.

The contribution of the oxidation, which is shown in Figure 7(c), is the one defining the THC light-off temperature from modelling. Analogously to CO, if the CDC is taken as baseline, $T50_{THC}$ is decreased by EGR and alternative fuels and deteriorated by dual-fuel combustion of diesel and propane. The minimum $T50_{THC}$ was also found for GTL-EGR and RME-EGR combustion with EGR at 144°C and 147°C (model) respectively. Although these THC light-off temperatures are almost identical, GTL-EGR showed the best THC light-off in contrast to CO abatament because of its highest HC-2 content (high reactivity) and lowest HC-3 (low reactivity). Concerning overall THC conversion efficiency (Figure 7(a)), the combination of adsorption and oxidation mechanisms at low temperature provided similar conversion efficiency till 150°C. However, the THC conversion efficiency is higher for GTL-EGR from this temperature on due to the better oxidation behaviour brought by its HC speciation.

Figure 8 shows the light-off curves of medium-heavy (HC-1) and light HCs (HC-2 and HC-3) respectively. The differences between combustion cases for each HC group were due to the oxidation inhibition terms for these species. This is a relevant difference with respect to THC conversion efficiency, which depends on the one of every species and the surrogate composition. The inhibition terms for every HC group are shown in Figure 9. Note that the calibration for light unsaturated (HC-2) coincided with CO (as proposed by Oh and Cavendish [34]) whilst HC-1 and HC-3 were calibrated differently. In fact, medium-heavy (HC-1) and light alkanes (HC-3) are less conditioned by NO than CO and light unsaturated HCs for low engine-out emissions (conventional combustion with diesel and alternative fuels) but are more sensitive to the increase of CO and THC emissions (dual-fuel combustion).

Despite the change in conversion efficiency of each HC group as a function of the combustion case, the THC conversion efficiency was clearly governed by the large differences in reactivity between each HC group. On the one hand, Figure 8(a) shows that the reactivity of HC-1 governed the THC conversion efficiency for conventional combustion cases. A relevant gap was observed with respect to low reactivity HCs (HC-3), represented by light alkanes and whose surrogate was propane. The light HCs conversion efficiency is shown in Figure 8(b). For the sake of easier understanding, light unsaturated HC and alkanes are plotted together for diesel-propane dual-fuel combustion cases. The reactivity of light alkanes (HC-3) is very low in comparison to both unsaturated (HC-2) and medium-heavy HCs (HC-1), as well as much more sensitive to the inhibition term (high difference between 0.2% and 0.5% propane cases). In rough terms, the $T50_{HC-3}$ is $100 - 150$°C higher than that of HC-1 and HC-2.

The negative impact on the conversion efficiency results found in dual-fuel combustion of diesel and propane were due to the high content in light HCs (non-adsorbable), being most of them alkanes belonging to the low reactivity group (HC-3). According to Figure 7, both 0.2% and 0.5% propane cases presented a bi-modal behaviour with flat THC conversion efficiency in the light-off region (between 40% and 60%) covering a wide temperature window that

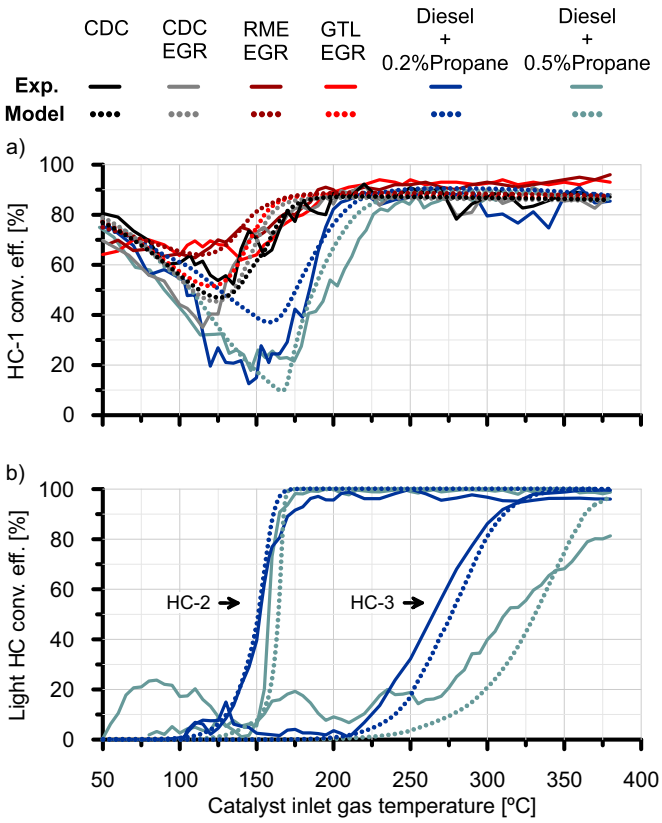

Figure 8: Comparison between experimental and modelled results: (a) Medium-heavy HC conversion efficiency and (b) light HC conversion efficiency.

ranged from 160°C to 275°C. This kind of response has been also found in other dual-fuel combustion strategies combining fuels of different reactivity, such as reactivity controlled compression ignition (RCCI) [5]. This fashion in THC conversion efficiency is justified by the HC speciation. On the one hand, the poor THC conversion efficiency at low temperature was caused by the low content in adsorbable HC species, which scarcely reached 13.6% for 0.2% propane case and fall to 8.8% when the injected propane increased to 0.5%. As pointed out by the experimental and modelling results represented in Figure 8, the oxidation of HCs did not start till ~ 150°C in dual-fuel combustion cases, when the light-off of light unsaturated HCs (HC-2 in Figure 8(b)) was reached. Medium-heavy HCs (HC-1 in Figure 8(a)) presented their light-off between 175°C (0.2% propane) and 187°C (0.5% propane). The delay in light-off of HC-1 group was due to the huge inhibition term of HCs in dual-fuel combustion cases (Figure 9) caused by the large engine-out CO and THC emissions. The light-off of light alkanes (HC-3) was moved forward in a relevant magnitude, to 275°C (0.2% propane) and 331°C (0.5% propane) as a function of the injected amount of propane. These high light-off temperatures for HC-3 and its majority content in dual-fuel combustion caused the bi-modal THC conversion efficiency representative of this combustion strategy.

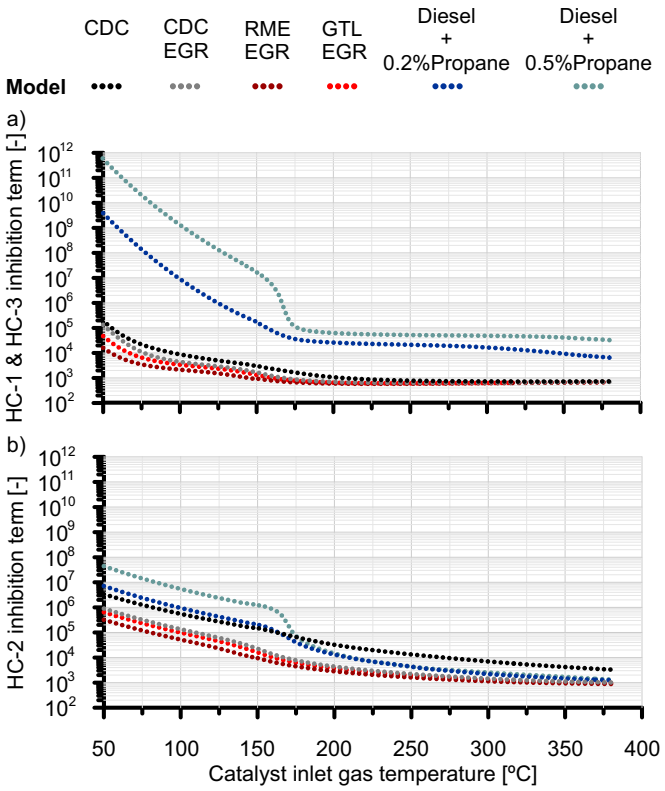

Figure 9: Oxidation inhibition term: (a) HC-1 & HC-3 groups and (b) HC-2 group.

Besides the evident penalty in THC conversion efficiency for dual-fuel combustion, it is interesting to analyse separately how the increase of the CO and THC engine-out emissions penalizes the HC oxidation in these working conditions. As discussed, CO and HCs are both strongly adsorpted on Pt sites affecting the auto-inhibition and competition between them [44]. To explore this dependence, the light-off test corresponding to the dual-fuel combustion with 0.2% propane was taken as baseline to assess the sensitivity to variations in engine-out CO and THC mole fraction. The exhaust gas composition of this case was modified increasing the CO and THC mole fraction in 1200 ppm independently. This way, each of these species reached similar values than the case of dual-fuel combustion with 0.5% propane. The original HC speciation shown in Figure 4 for dual-fuel combustion with 0.2% propane was kept constant. Figure 10 shows the results for the conversion efficiency of HC-2 (top chart) and HC-3 (bottom chart) groups.

Comparing the light-off curves, the increase of CO mole fraction presented different effects on each HC. The HC-2 light-off was delayed 15°C and became similar to that corresponding to 0.5% propane. As a remark, CO light-off would be affected similarly since the model setup revealed that the inhibition dependence was found equivalent for CO and HC-2. By contrast, positive impact on HC-3 light-off was noticed due to CO complete oxidation at the temperature range at which HC-3 starts to be burnt out. The variation in the light-off curve is due to the differences

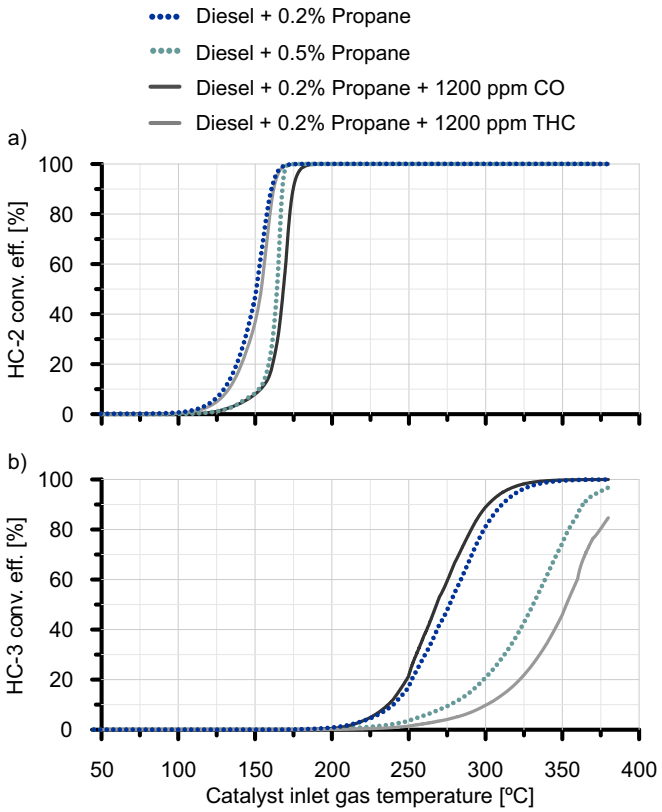

Figure 10: Conversion efficiency results of the parametric study for (a) HC-2 group and (b) HC-3 group.

in the substrate temperature, in the inhibition terms because of residual CO washcoat mole fraction and in the mass transfer coefficients due to change in the inlet gas composition.

Similar to CO influence, the increase of THC engine-out emission had different effects on low and high reactivity HC groups. Light unsaturated HCs (HC-2) suffered a negligible variation of its reactivity. This is in agreement with the slight change in experimental and modelled results from 0.2% to 0.5% propane combustions shown in Figure 8(b) for HC-2 (increase in CO governing the light-off delay). Thus, the CO content controls the THC conversion efficiency at low temperature in dual-fuel combustion cases combining diesel and propane. However, the light-off of light alkanes (HC-3) was very sensitive to the increase in THC. Again, these results contribute to explain the experimental variation observed in HC-3 light-off when varies the propane content in the combustion. In this particular case, the THC increase determined the worsening of the HC-3 light-off and, hence, the deterioration of the THC conversion efficiency at high temperature.

4. Conclusions

The pollutants' abatement performance of an oxidation catalyst working under actual exhaust gas compositions generated by a variety of fuels and combustion strategies was examined. The studied cases covered the use of CDC (with EGR effect), RME, GTL and diesel-propane dual-fuel combustion. New comprehensive understanding of the interactions between exhaust species has been generated thanks to the combination of experimental and modelling results. The calibration of the catalytic reactions' chemical kinetic parameters enables to quantify the importance of the interaction between the species composing the exhaust gas on the catalyst reactivity and, in particular, in the light-off temperature.

The experimental and model results showed that CO light-offs are governed by species' inhibition. The lowest CO light-off temperature is reached when combining alternative fuels with EGR because of their low CO, THC and NO engine-out emissions. Comparing the catalyst response under CDC with and without EGR (resultant in high and low engine-out NO emission) and the single-fuel (diesel, RME, GTL) cases demonstrate the NO inhibition effects on the CO (and THC) light-offs. The high NO mole fraction in CDC determined the highest CO inhibition term because of competition for the catalyst's active sites. Being the usage of EGR positive for the catalyst performance, short-route EGR is preferable in cold start conditions since it also contributes to higher space velocities in the catalyst. The diesel-propane dual-fuel combustion obtained the worst CO light-off mainly because of the large CO and THC engine-out emission.

In the case of the THC light-off, the role of inhibition appeared combined with the influence of the HC composition and adsorption. High reactivity HCs were clearly distinguished from low reactivity one in the light-off tests. Medium-heavy HCs and light alkanes are less inhibited than unsaturated light HCs (and CO) for low engine-out emissions (single-fuel combustion), but they are more penalised by the increase of THC and CO emissions (dual-fuel combustion). Thus, the alternative fuels also confirmed the best catalyst performance for THC, with good adsorption conversion efficiency due to the high content in medium-heavy HCs and the lowest light-off temperature. Similarly to CO light-off, the boundaries imposed by the dual-fuel combustion led also to the worst performance in THC abatement. The large CO and THC engine-out emissions and high species' inhibition rates were partially responsible of the light-off delay with respect to the single-fuel combustion. The THC speciation also penalised the abatement of THC. The high percentage content of light alkanes gave as a result a bi-modal light-off curve, while the adsorption contribution was negligible because of the low content of medium-heavy HCs. The kinetic limitations resulted very sensitive to the propane content in the combustion process lowering the reaction rate at low temperature because of competition with CO and at high temperature because of the HC self-inhibition.

This work demonstrates how the combination of experimental and modelling results enables to understand catalyst performance to abate emissions. Therefore, it is a powerful tool to predict potential synergies between fuels, combustion modes and exhaust aftertreatment components to guide the design of clean and efficient fuels/combustion/aftertreatment

as a system level. Particularly, the engine-out emission benefits on the catalyst conversion efficiency performance from the utilisation of alternative fuels have been evidenced and understood.

Acknowledgements

This research has been partially supported by FEDER and the Government of Spain through project TRA2016-79185-R and by Universitat Politècnica de València under a grant with reference number FPI-2018-S2-10 to the Ph.D. student María José Ruiz.

References

[1] Jiang Y, Zhao H, Liang J, Yue L, Li T, Luo Y, Liu Q, Lu S, Asiri AM, Gong Z, Sun X. Anodic oxidation for the degradation of organic pollutants: Anode materials, operating conditions and mechanisms. A mini review. Electrochem. Commun. 2021;123:106912. https://doi.org/10.1016/j.elecom.2020.106912.

[2] Machado CP, Machado M, Santos MC. Coupling photocatalytic degradation using a green TiO_2 catalyst to membrane bioreactor for petroleum refinery wastewater reclamation. J. Water Process. Eng. 2020;34:101093. https://doi.org/10.1016/j.jwpe.2019.101093.

[3] Joshi A. Review of vehicle engine efficiency and emissions, in: SAE Technical Paper 2020;2020-01-0352. https://doi.org/10.4271/2020-01-0352.

[4] Rappé KG, DiMaggio C, Pihl JA, Theis JR, Oh SH, Fisher GB, Parks J, Easterling VG, Yang M, Stewart ML, Howden KC. Aftertreatment protocols for catalyst characterization and performance evaluation: low-temperature oxidation, storage, three-way, and NH_3-SCR catalyst test protocols. Emission Contr. Sci. Technol. 2019;5:183-214. https://doi.org/10.1007/s40825-019-00120-7.

[5] Piqueras P, García A, Monsalve-Serrano J, Ruiz MJ. Performance of a diesel oxidation catalyst under diesel-gasoline reactivity controlled compression ignition combustion conditions. Energy Convers. Manag. 2019;196:18-31. https://doi.org/10.1016/j.enconman.2019.05.111.

[6] Bhardwaj OP, Blanco-Rodriguez D, Krishnamurthy K, Holderbaum B. Optimization of engine efficiency and diesel aftertreatment system architecture using an integrated system simulation approach. SAE Technical Paper 2016;2016-28-0227. https://doi.org/10.4271/2016-28-0227.

[7] Ren S, Wang B, Zhang J, Wang Z, Wang, J. Application of dual-fuel combustion over the full operating map in a heavy-duty multi-cylinder engine with reduced compression ratio and diesel oxidation catalyst. Energy Convers. Manag. 2018;166:1-12. https://doi.org/10.1016/j.enconman.2018.04.011.

[8] Ashok B, Nanthagopal K, Anand V, Aravind KM, Jeevanantham AK, Balusamy S. Effects of n-octanol as a fuel blend with biodiesel on diesel engine characteristics. Fuel 2019;235:363-373. https://doi.org/10.1016/j.fuel.2018.07.126.

[9] García A, Piqueras P, Monsalve-Serrano J, Sari RL. Sizing a conventional diesel oxidation catalyst to be used for RCCI combustion under real driving conditions. Appl. Therm. Eng. 2018;140:62-72. https://doi.org/10.1016/j.applthermaleng.2018.05.043.

[10] Napolitano P, Fraioli V, Guido C, Beatrice C. Assessment of optimized calibrations in minimizing GHG emissions from a dual fuel NG/Diesel automotive engine. Fuel 2019;258:115997. https://doi.org/10.1016/j.fuel.2019.115997.

[11] Benajes J, García A, Monsalve-Serrano J, Sari RL. Clean and efficient dual-fuel combustion using OMEx as high reactivity fuel: comparison to diesel-gasoline calibration. Energy Convers. Manag. 2020;216:112953. https://doi.org/10.1016/j.enconman.2020.112953.

[12] Bogarra M, Herreros JM, Tsolakis A, York APE, Millington PJ. Study of particulate matter and gaseous emissions in gasoline direct injection engine using on-board exhaust gas fuel reforming. Appl. Energy 2016;180:245-255. https://doi.org/10.1016/j.apenergy.2016.07.100.

[13] Raman LA, Deepanraj B, Rajakumar S, Sivasubramanian V. Experimental investigation on performance, combustion and emission analysis of a direct injection diesel engine fuelled with rapeseed oil biodiesel. Fuel 2019;246:69-74. https://doi.org/10.1016/j.fuel.2019.02.106.

[14] El Shenawy EA, Elkelawy M, Bastawissi HA-E, Panchal H, Shams MM. Comparative study of the combustion, performance, and emission characteristics of a direct injection diesel engine with a partially premixed lean charge compression ignition diesel engines. Fuel 2019;249:277-285. https://doi.org/10.1016/j.fuel.2019.03.073.

[15] Tuner M. Review and benchmarking of alternative fuels in conventional and advanced engine concepts with emphasis on efficiency, CO_2, and regulated emissions. SAE Tech. Pap. 2016;2016-01-0882. https://doi.org/10.4271/2016-01-0882.

[16] Kluschke P, Gnann T, Plötz P, Wietschel M. Market diffusion of alternative fuels and powertrains in heavy-duty vehicles: a literature review. Energy Rep. 2019;5;1010–1024. https://doi.org/10.1016/j.egyr.2019.07.017.

[17] Heuser B, Schnorbus T, Müther M, Lindemann B. Closed carbon cycle mobility: pathways towards a CO_2 neutral mobility. FEV Diesel Powertrains 3.0 Conference, Rouen, France, July 2019.

[18] den Boer E, Aarnink S, Kleiner F, Pagenkopf J. Zero emissions trucks: an overview of state-of-the-art technologies and their potential. Delft, CE Delft, July 2013.

[19] Hassaneen A, Munack A, Ruschel Y, Schroeder O, Krahl J. Fuel economy and emission characteristics of Gas-to-Liquid (GTL) and Rapeseed Methyl Ester (RME) as alternative fuels for diesel engines. Fuel 2012;97:125-130. https://doi.org/10.1016/j.fuel.2012.01.077.

[20] Novakovic M, Shamun S, Malmborg VB, Kling KI, Kling J, Vogel UB, Tunestal P, Pagels J, Tuner M. Regulated emissions and detailed particle characterisation for diesel and RME biodiesel fuel combustion with varying EGR in a heavy-duty engine. SAE Technical Paper 2019;2019-01-2291. https://doi.org/10.4271/2019-01-2291.

[21] Hammoudi M, Gruel DN, Charlet A, Chamaillard Y. Effect of optimizing of the start of injection timing for improving NOx/PM trade-off in DI diesel engine fueled with rapeseed methyl ester. SAE Technical Paper 2020;2020-01-2132. https://doi.org/10.4271/2020-01-2132.

[22] Rounce P, Tsolakis A, York APE. Speciation of particulate matter and hydrocarbon emissions from biodiesel combustion and its reduction by aftertreatment. Fuel 2012;96:90-99. https://doi.org/10.1016/j.fuel.2011.12.071.

[23] Sampara CS, Bissett EJ, Chmielewski M. Global kinetics for a commercial diesel oxidation catalyst with two exhaust hydrocarbons. Ind. Eng. Chem. Res. 2008;47:311-322. https://doi.org/10.1021/ie070813x.

[24] AL-Harbi M, Hayes R, Votsmeier M, Epling WS. Competitive no, co and hydrocarbon oxidation reactions over a diesel oxidation catalyst. Can J Chem Eng 2012;90:1527-1538. https://doi.org/10.1002/cjce.20659.

[25] Daneshvar K, Dadi RK, Luss D, Balakotaiah V, Kang SB, Kalamaras CM, Epling WS. Experimental and modeling study of CO and hydrocarbons light-off on various Pt-Pd/ γ-Al_2O_3 diesel oxidation catalysts. Chem. Eng. J. 2017;323:347-360. https://doi.org/10.1016/j.cej.2017.04.078.

[26] Patterson MJ, Angove DE, Cant NW. The effect of carbon monoxide on the oxidation of four C_6 to C_8 hydrocarbons over platinum, palladium and rhodium. Appl. Catal. B 2000;26:47-57. https://doi.org/10.1016/S0926-3373(00)00110-7.

[27] Lafossas F, Matsuda Y, Mohammadi A, Morishima A, Inoue M, Kalogirou M, Koltsakis G, Samaras Z. Calibration and validation of a diesel oxidation catalyst model: from synthetic gas testing to driving cycle applications. SAE Technical Paper 2011;2011-01-1244. https://doi.org/10.4271/2011-01-1244.

[28] Storey JME, Curran SJ, Lewis SA, Barone TL, Dempsey AB, Moses-DeBusk M, Hanson RM, Prikhodko VY, Northrop WF. Evolution and current understanding of physicochemical characterization of particulate matter from reactivity controlled compression ignition combustion on a multicylinder light-duty engine. Int J Engine Res 2016;18:505-519. https://doi.org/10.1177/1468087416661637.

[29] Lefort I, Herreros JM, Tsolakis A. Reduction of low temperature engine pollutants by understanding the exhaust species interactions in a diesel oxidation catalyst. Environ. Sci. Technol. 2014;48:2361-2367. https://doi.org/10.1021/es4051499.

[30] Payri F, Arnau FJ, Piqueras P, Ruiz MJ. Lumped approach for flow-through and wall-flow monolithic reactors modelling for real-time automotive applications. SAE Technical Paper 2018;2018-01-0954. https://doi.org/10.4271/2018-01-0954.

[31] Galindo J, Serrano JR, Piqueras P, García-Afonso Ó. Heat transfer modelling in honeycomb wall-flow diesel particulate filters. Energy 2012;43:201-213. https://doi.org/10.1016/j.energy.2012.04.044.

[32] Depcik C, Assanis D. One-dimensional automotive catalyst modeling. Prog. Energy Combust. Sci. 2005;31:308-369. https://doi.org/10.1016/j.pecs.2005.08.001.

[33] Poling BE, Prausnitz JM, O'connell JP. The properties of gases and liquids, Fifth edition. McGraw-Hill Education; New York, 2001. ISBN 9780070116825.

[34] Oh SH, Cavendish JC. Transients of monolithic catalytic converters. Response to step changes in feedstream temperature as related to controlling automobile emissions. Ind Eng Chem Prod Res Dev 1982;21:29-37. https://doi.org/10.1021/i300005a006.

[35] Kryl D, Kočí P, Kubíček M, Marek M, Maunula T, Härkönen M. Catalytic converters for automobile diesel engines with adsorption of hydrocarbons on zeolites. Ind. Eng. Chem. Res. 2005;44:9524-9534. https://doi.org/10.1021/ie050249v.

[36] Siegl WO, Hammerle RH, Herrmann HM, Wenclawiak BW, Luers-Jongen B. Organic emissions profile for a light-duty diesel vehicle. Atmospheric Environ. 1999;33:797-805. https://doi.org/10.1016/S1352-2310(98)00209-X.

[37] Payri F, Bermúdez VR, Tormos B, Linares WG. Hydrocarbon emissions speciation in diesel and biodiesel exhausts. Atmospheric Environ. 2009;43:1273-1279. https://doi.org/10.1016/j.atmosenv.2008.11.029.

[38] Shen VK, Siderius DW, Krekelberg WP, Hatch HW. NIST Standard Reference Simulation Website, NIST Standard Reference Database Number 173. National Institute of Standards and Technology, Gaithersburg MD, 20899.

[39] Majer V, Svoboda V. Enthalpies of vaporization of organic compounds: A critical review and data compilation. Oxford: Blackwell Science Publications; 1985.

[40] Scott DW. Chemical thermodynamic properties of hydrocarbons and related substances: Properties of the alkane hydrocarbons, C1 through C10, in the ideal gas state from 0 to 1500K. US Bureau of Mines 1974.

[41] Chao J, Zwolinski BJ. Ideal gas thermodynamic properties of ethylene and propylene. J Phys Chem Ref Data 1975;4:251. https://doi.org/10.1063/1.555518.

[42] van Steen E, Callanan LH, Claeys M. Recent advances in the science and technology of zeolites and related materials. Elsevier Science 2004.

[43] De Moor BA, Ghysels A, Reyniers MF, Speybroeck VV, Waroquier M, Marin GB. Normal mode analysis in zeolites: toward an efficient calculation of adsorption entropies. J. Chem. Theory Comput. 2011;7:1090-1101. https://doi.org/10.1021/ct1005505.

[44] Diehl F, Jr. JB, Duprez D, Guibard I, Mabilon G. Catalytic oxidation of heavy hydrocarbons over Pt/Al_2O_3. Influence of the structure of the molecule on its reactivity. Appl. Catal. B 2010;95:217-227. https://doi.org/10.1016/j.apcatb.2009.12.026.

Nomenclature

Acronyms

ATS	Aftertreatment system
CDC	Conventional diesel combustion
CO	Carbon monoxide
CO_2	Carbon dioxide
EGR	Exhaust gas recirculation
FTIR	Fourier-transform infrared spectroscopy
GTL	Gas to liquid
HC	Hydrocarbon
LHV	Lower heating value
NO	Nitric oxide
NO_2	Nitrogen dioxide

NOx	Nitrogen oxides
PGM	Platinum group metal
RCCI	Reactivity controlled compression ignition
RME	Rapeseed methyl ester
THC	Total hydrocarbons
ULSD	Ultra low sulphur diesel

Latin letters

a_{H_f}	Correlation coefficient of enthalpy of formation
a_n	First-order solution constant of species n
A	Area
b_n	Zero-order solution constant of species n
c_p	Specific heat
C	Equivalent thermal capacitance
D_h	Hydraulic diameter
D_m	Molecular diffusivity
E_a	Activation energy
G	Inhibition term
H_f	Enthalpy of formation
k_m	Mass transfer coefficient
k_r	Kinetic constant of reaction r
K_i	Inhibition term coefficient i
$\dot{m}$	Mass flow
M	Molecular weight
$\dot{n}_{gas}$	Exhaust gas mole flow
p	Pressure
P_f	Pre-exponential factor
$\dot{q}_{ht}$	Gas to wall thermal power
$\dot{q}_r$	Reaction power
R	Equivalent thermal resistance
R_n	Reaction rate of species n
$\Re$	Universal gas constant
S_p	Specific surface
Sh	Sherwood number
T	Temperature

T_c	Critical temperature
T50	Light-off temperature
u	Velocity
x	Axial coordinate
X	Mole fraction
Y	Mass fraction

Greek letters

$\Delta H_{\frac{ads}{des}}$	Adsorption-desorption enthalpy
Δt	Time-step
θ	Surface coverage
υ	Diffusion volume
ν	Stoichiometric coefficient
τ	Residence time
ψ	Specific storage capacity
Ψ	Storage capacity

Subscripts

ads	Adsorption
des	Desorption
fur	Furnace
gas	Exhaust gas flow
in	Inlet
n	Species
out	Outlet
ox	Oxidation
rad	Radial
red	Reduction
w	Substrate
wc	Washcoat